

# Macroscopic production of highly nuclear-spin-polarized molecules from IR-excitation and photodissociation of molecular beams

C. S. Kannis<sup>1,2</sup> and T. P. Rakitzis<sup>2,3,\*</sup>

<sup>1</sup>*Institute for Nuclear Physics, Forschungszentrum Jülich, 52425 Jülich, Germany*

<sup>2</sup>*University of Crete, Department of Physics, Herakleio, Greece*

<sup>3</sup>*Foundation for Research and Technology Hellas, Institute of Electronic Structure and Laser, N. Plastira 100, Heraklion, Crete, Greece, GR-71110*

(Dated: March 2, 2022)

Pure, highly nuclear-spin-polarized molecules have only been produced with molecular beam-separation methods, with production rates up to  $\sim 3 \times 10^{12} \text{ s}^{-1}$ . Here, we propose the production of isotopes of spin-polarized hydrogen ( $\text{H}_2$ ,  $\text{D}_2$ , HD, DT) and water ( $\text{H}_2\text{O}$ ,  $\text{D}_2\text{O}$ ) at rates of  $\sim 10^{21} \text{ s}^{-1}$ , from the IR-excitation and photodissociation of molecular beams of formaldehyde ( $\text{CH}_2\text{O}$ ) and formic acid ( $\text{CH}_2\text{O}_2$ ), respectively. These macroscopic quantities are sufficient for NMR signal enhancement, and for the needs of a nuclear fusion reactor, to increase the D-T or D- $^3\text{He}$  unpolarized nuclear fusion cross section by  $\sim 50\%$ .

The production of nuclear spin polarization is important in several fields, including the study of spin-dependent effects in particle and nuclear physics [1], and in applications of nuclear magnetic resonance (NMR) [2–4]. However, current methods for producing highly spin-polarized molecules, such as molecular-beam separation techniques, polarization through “brute force” cryogenic cooling, dynamic nuclear polarization (DNP), and pulsed-laser excitation of molecular beams, have significant production and polarization limitations for many applications.

“Brute force” cryogenic cooling of solid  $\text{D}_2$  to 35 mK in a 14.5 T field, produces a polarization of only about 13% [5]. For 100% polarized nuclei, The D-T and D- $^3\text{He}$  nuclear-fusion reaction cross sections are enhanced by 50% [6], and may increase the reactor efficiency by  $\sim 75\%$  [7]. A GW nuclear fusion reactor will need  $\sim 10^{21} \text{ s}^{-1}$  of 100% polarized D to benefit fully from this effect [8–10]. Therefore, the “brute force” method cannot produce sufficiently polarized D for this application.

In DNP, the unpaired electrons in free radicals are highly polarized at low temperature in a magnetic field, and this polarization is transferred to the nuclei of the target sample [11]. This works successfully for a wide range of molecules, however the removal of the radicals, necessary for *in vivo* NMR applications, is difficult and can significantly lower the sample polarization [12].

Molecular-beam separation techniques, using electric or magnetic field gradients, is the only method that can produce pure,  $\sim 100\%$  nuclear-spin-polarized molecules, however only microscopic production rates have been demonstrated of  $\sim 3 \times 10^{12}$  for ortho- $\text{H}_2$  and  $\sim 5 \times 10^{11} \text{ s}^{-1}$  for ortho- $\text{D}_2$  [13], and below  $\sim 10^9$  for ortho- $\text{H}_2\text{O}$  [14, 15], many orders of magnitude lower than required for many applications; for example, NMR applications and tests of polarized fusion require production rates of at least  $10^{17} \text{ s}^{-1}$ .

The single-photon rovibrational excitation of molecular beams with an IR laser pulse [16, 17], followed by

transfer of the rotational polarization to the nuclear spin via the hyperfine interaction, has been shown to polarize highly the nuclear spins of isolated molecules. This method of hyperpolarization has been demonstrated for Cl nuclei in HCl molecules [18, 19]. However, a path for high production rates for important nuclei, such as H/D/T, was not shown; also, high polarization was not demonstrated for H isotopes via IR excitation, as the rotational polarization preferentially polarizes the more strongly coupled Cl nucleus first. The biggest problem is that only isolated spin-polarized atoms have been produced with this method, and that the production of spin-polarized molecules (such as  $\text{H}_2$  isotopes) have only been performed by recombining the polarized atoms at a surface [20]; this is a very complicated extra step, which has not been demonstrated at high production rates.

Here, we propose breakthroughs to the rovibrational excitation method that will allow macroscopic production rates of pure, highly-polarized molecules ( $\sim 100\%$ ), at rates  $\sim 10^{20} \text{ s}^{-1}$  for a tabletop setup, and of at least  $\sim 10^{21} \text{ s}^{-1}$  for an industrial-scale setup, motivated by the recent availability of tabletop tunable, narrow-bandwidth, high-power IR lasers, producing  $\sim 10^{21} \text{ photons s}^{-1}$  [21]. These breakthroughs are: (i) optical excitation steps that allow *only* molecules with 100% nuclear polarization to be photodissociated, providing a pure polarization spin filter, and (ii) excitation and polarization of larger molecules which can be photodissociated to yield exclusively polarized molecular photofragments, without needing to recombine polarized atoms; this is particularly important for molecules that are not IR active (such as  $\text{H}_2$  isotopes), and cannot be excited directly. Specifically, we propose the IR-excitation of the special cases of formaldehyde ( $\text{CH}_2\text{O}$ ) or formic acid ( $\text{CH}_2\text{O}_2$ ), which can be photodissociated to yield exclusively the  $\text{H}_2 + \text{CO}$  [22] or  $\text{H}_2\text{O} + \text{CO}$  [23] channels, respectively. The target molecules (here  $\text{H}_2$  or  $\text{H}_2\text{O}$  isotopes) can then be selectively trapped at a surface. Thus, we propose the production of macroscopic quantities of  $\sim 100\%$  nuclear-

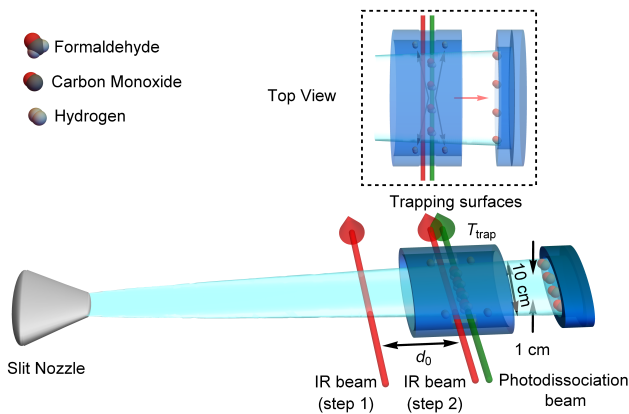


FIG. 1. Experimental setup: supersonic expansion of  $\text{CH}_2\text{O}$  or  $\text{CH}_2\text{O}_2$  gas, followed by IR excitation (step 1), time evolution for time  $t_{max} = d_0/v$ , then photodissociation, and trapping of polarized hydrogen or water photofragments at the cold surface.

spin-polarized isotopes of hydrogen molecules ( $\text{H}_2$ , HD, DT) and water molecules ( $\text{H}_2\text{O}$ ,  $\text{D}_2\text{O}$ ), sufficient for the demanding applications in polarized nuclear fusion and NMR signal enhancement.

Below, and in Figs. 1 and 2, we give details on the production of 100% nuclear-spin-polarized molecules from IR-excitation and photodissociation of  $\text{CH}_2\text{O}$  and  $\text{CH}_2\text{O}_2$ . The steps are described generally, but specific numbers are given for the case of  $\text{CH}_2\text{O}$  (for production rates of  $10^{20} \text{ s}^{-1}$  spin-polarized  $\text{H}_2$ ):

1. *Slit nozzle supersonic expansion.* Produces a  $10 \text{ cm} \times 1 \text{ cm}$  jet (Fig. 1), with  $\text{CH}_2\text{O}$  density of  $2 \times 10^{15} \text{ cm}^{-3}$  (seeded in He) with beam velocity of  $2 \times 10^5 \text{ cm s}^{-1}$ , translational temperature of  $\sim 0.1 \text{ K}$  and rotational temperature of  $\sim 1 \text{ K}$ , thus cooling  $\sim 90\%$  of the  $\text{CH}_2\text{O}$  to the ground  $J = 0$  state [24–27].

2. *IR excitation (step 1).* Transition from the ground state  $|\nu = 0, J = 0, m_J = 0\rangle$  to  $|\nu', J, m_J = +J\rangle$  with  $\sigma_+$  light, and  $J = 1$  or  $2$  (Fig. 2).  $J = 1$  is used for photoproducts with total nuclear spin  $I = 1$  (such as ortho  $\text{H}_2$  or  $\text{H}_2\text{O}$ ), and  $J = 2$  for nuclei with total nuclear spin  $I = 3/2$  (such as HD or DT) or  $2$  (such as ortho  $\text{D}_2$  or  $\text{D}_2\text{O}$ ), via successive two-photon absorption using STIRAP [28–30], for which population-transfer efficiency is typically  $> 90\%$ . The absorption cross sections are  $\sim 10^{-16} \text{ cm}^2$  (for  $\nu' = \nu_2\nu_5$  at  $4581.69 \text{ cm}^{-1}$ ) and the column density of the ground state is  $3 \times 10^{16} \text{ cm}^{-2}$  so that greater than  $99\%$  of the  $10^{21} \text{ s}^{-1}$  IR photons are absorbed (as the  $1 \text{ MHz}$  laser linewidth is much narrower than the transition linewidth).

3. *Hyperfine polarization beating.* Subsequently, we leave the system to evolve freely, transferring rotational polarization to nuclear polarization, until the population of  $|\nu', J, m_J = -J\rangle$  (for  $I = 1$  or  $2$ ) or  $|\nu', J, m_J = -J+1\rangle$  (for  $I = 3/2$ ) is maximized ( $t = t_{max}$ ). This state

is 100% nuclear-spin polarized, due to the conservation of the total angular momentum projection along the quantization axis (hyperfine beatings under similar conditions have been demonstrated for HCl, HD,  $\text{D}_2$  [18, 31, 32]). For  $\text{CH}_2\text{O}$ , 16% of the population is 100% nuclear-spin-polarized and is transferred to the  $m_J = -1$  state. The total rotational energy transfer and depolarization cross section for the  $|J = 1, K = 0, M = 1\rangle$  state in  $\text{CH}_2\text{O}$  is  $\sim 3 \times 10^{-15} \text{ cm}^2$  [33] (assuming a collision-energy-independent cross section). For collisional speeds of  $\sim 10^3 \text{ cm s}^{-1}$ , the de-excitation rate is  $\sim 3 \times 10^{-12} \text{ cm}^3 \text{ s}^{-1}$ , which, for  $10^{15} \text{ cm}^3$  densities, gives a de-excitation time of  $\sim 300 \mu\text{s}$ ; therefore,  $t_{max}$  should be significantly less than  $300 \mu\text{s}$ .

4. *Hyperfine beating stopped.* At  $t = t_{max}$ , the beam enters a magnetic field of  $1 \text{ mT}$ , which stops the hyperfine beating [34].

5. *IR excitation (step 2) and photodissociation.* The transition  $|\nu', J, m_J = -J\rangle \rightarrow |\nu'', J = 0, m_J = 0\rangle$  (for  $I = 1$  or  $2$ ) or the  $|\nu', J, m_J = -1\rangle \rightarrow |\nu'', J = 1, m_J = +1\rangle$  (for  $I = 3/2$ ), with  $\sigma_+$  light, so that only the 100% nuclear-spin-polarized state is excited to the highest level. This fully-polarized state is then exclusively photodissociated by the photolysis laser (the lower states not having enough energy to photodissociate). For  $\text{CH}_2\text{O}$  column density of  $3 \times 10^{16} \text{ cm}^{-2}$  and a photodissociation cross section of  $2.5 \times 10^{16} \text{ cm}^2$  (Fig. 4), more than 99% of the molecules are photodissociated, for laser fluxes of  $2 \times 10^{20} \text{ photons cm}^{-2} \text{ s}^{-1}$ . The photodissociation cross section for higher vibrational states is shifted to the green from the UV, due to the IR absorption energy of  $\sim 1 \text{ eV}$ . The photodissociation cross section of formic acid at  $248 \text{ nm}$ , for the  $\text{CO} + \text{H}_2\text{O}$  channel, is about 1000 times smaller [35, 36], therefore a buildup cavity will be needed for the photodissociation laser, at  $355 \text{ nm}$  (for 2 IR photons) or  $450 \text{ nm}$  (for 4 IR photons), to absorb a large percentage of the photolysis light. The produced  $\text{H}_2$  molecules are in  $J$  states peaking at  $\sim 3$  [37], and hence a static magnetic field of  $\sim 1 \text{ T}$  is applied in the photodissociation region to prevent significant polarization exchange with  $J$  [38].

6. *Cold trapping.* More than 90% of the hydrogen or water isotopes reach trapping surfaces (that cover more than 90% of  $4\pi$  steradians), and are selectively trapped at these cold trapping surfaces with unity sticking probability [39] (the CO mainly follows the beam direction and is trapped elsewhere, with the unphotodissociated molecules (Fig. 1)).

The product of the efficiencies of the above steps 1-6 is at least 10%. Therefore,  $10^{21} \text{ IR photons s}^{-1}$  will produce and trap at least  $10^{20} \text{ s}^{-1}$  spin-polarized molecules, and can be scaled up with larger laser powers and slit lengths.

We describe in more detail why this method surpasses conventional methods by several orders of magnitude. Conventional molecular-beam separation methods are based on the differential deflection of the spin-

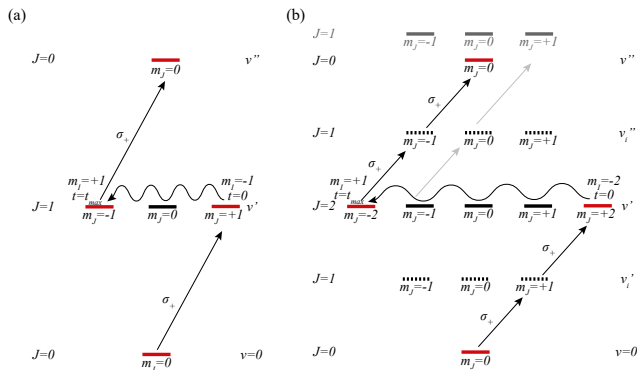


FIG. 2. Excitation schemes for production of nuclear spin-polarized molecules with (a)  $I = 1$  (e.g. with constituent atoms of D or  $H_2$ ), and (b)  $I = 3/2$  or 2 (e.g. for HD, DT or  $D_2$ ). The squiggly arrows show rotational polarization reduction  $\Delta m_J = -2$  or  $-4$ , associated with nuclear spin increase  $\Delta m_I = +2$  or  $+4$  (for Figs. 2(a) or 2(b), respectively). Only 100% nuclear-spin-polarized molecules reach the upper state.

projection states, from a beam with a cross sectional area  $A$ , velocity  $v$ , and density  $\rho$ , with large, localized B-field or E-field gradients, which limit  $A \sim 1 \text{ cm}^2$  to be small and localized. However, the beam density must be low enough so that the beam divergence, from collisions, is less than the differential deflections of the target spin-projection states. This constraint limits the beam density to  $\rho \sim 10^{11} \text{ cm}^{-3}$  for open-shell atoms [40]. The beam separation occurs over a distance of  $\sim 1 \text{ m}$  and on the ms timescale, with a beam velocity  $v$  typically in the range  $0.2\text{--}2.5 \times 10^5 \text{ cm/s}$ . The largest production rate (given by  $Av\rho$ ) for spin-polarized H atoms, which is the most favorable case, has been  $\sim 5 \times 10^{16} \text{ H/s}$  [40]. For closed-shell molecules, the production rates are several orders of magnitude lower (as nuclear magnetic moments are  $\sim 10^3$  times smaller than electronic ones, due to the  $\sim 10^3$  larger mass).

In contrast, the polarization of nuclear spins in a molecular beam, via the IR-excitation method, occurs by the intramolecular transfer of rotational to nuclear polarization, via the hyperfine interaction on the  $\mu\text{s}$  timescale, and thus does not require any type of beam separation or external inhomogeneous static fields. The lack of need to spatially separate the spin-states in the molecular beam, the shorter polarization time, and the ability to use a long slit expansion (not possible for conventional beam-separation methods due to the inhomogeneous fields), allow the beam area  $A$  and density  $\rho$  to be much higher than for beam-separation methods, e.g.  $A \sim 10\text{--}1000 \text{ cm}^2$ , and  $\rho \sim 10^{15} \text{ cm}^{-3}$ , which are 1-3 and 4 orders of magnitude higher, respectively. This increase in  $A$  and  $\rho$  potentially allows a total production rate  $Av\rho$  of up to  $\sim 10^{23} \text{ s}^{-1}$ . The production rate is limited by the absorbed photons for the IR-excitation and photodissocia-

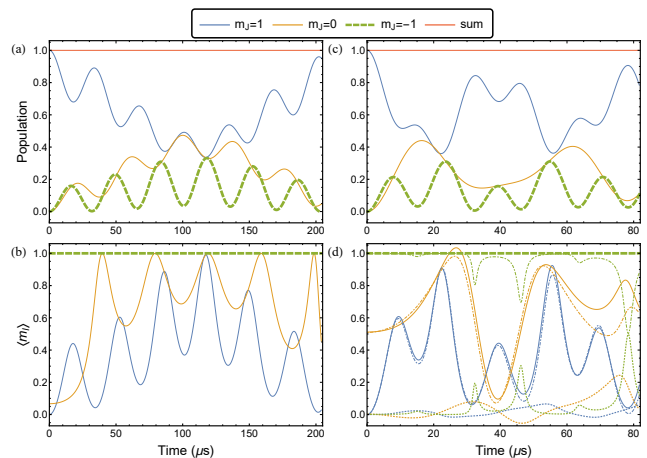


FIG. 3.  $\text{CH}_2\text{O}$  (a,b): Population and  $\langle m_I \rangle$  of  $m_J$  states as function of time. The  $m_J = -1$  state reaches 15.9% of the total population at  $\sim 16.2 \mu\text{s}$ .  $\text{CHDO}$  (c,d): Population and  $\langle m_I \rangle$  of  $m_J$  states as function of time. The solid lines (and the dashed thick line) correspond to the total nuclear spin projection, whereas the dash-dotted and dotted lines correspond to  $\langle m_{ID} \rangle$ , and  $\langle m_{IH} \rangle$  respectively. The  $m_J = -1$  state reaches 21.4% of the total population at  $7.9 \mu\text{s}$ . By that time, mainly the deuterium is polarized.

tion steps: tabletop IR-excitation and photodissociation lasers producing  $\sim 10^{21}$  photons  $\text{s}^{-1}$  are available commercially; industrial-scale lasers can reach  $10^{23} \text{ s}^{-1}$ . We note that related arguments were used to predict the production of ultrahigh densities of spin-polarized hydrogen (SPH) atoms from hydrogen halide photodissociation [41], and indeed  $10^{19}\text{--}10^{20}$  SPH were observed [42–44], 8-9 orders higher than those from beam separation methods; therefore surpassing conventional methods by many orders of magnitude is not unprecedented.

The IR-excitation method depends crucially on transferring a large fraction of the population to the 100% nuclear-spin-polarized state, and in short enough time ( $t_{max} \lesssim 30 \mu\text{s}$ ) to avoid significant depolarization under these conditions. Below, we give a description of the calculation of the polarization transfer and  $t_{max}$  for  $\text{CH}_2\text{O}$  and  $\text{CH}_2\text{O}_2$  isotopes.

The  $\text{CH}_2\text{O}$  ortho states ( $I = 1$ ) are described by  $K_{-1} = 1, 3, 5, \dots$  and the para states by  $K_{-1} = 0, 2, 4, \dots$  in the notation  $J_{K_{-1}K_1}$  [45]. The hyperfine hamiltonian matrix elements of the  $J = 1, K_{-1} = 1$  state can be written as [46]:

$$E/h = C(-1)^{I+J+F} [I(I+1)(2I+1)J(J+1)(2J+1)]^{1/2} \times \left\{ \begin{matrix} F & I & J \\ 1 & J & I \end{matrix} \right\} + D(-1)^{I+J+F} \left\{ \begin{matrix} F & I & J \\ 2 & J & I \end{matrix} \right\} \times \left[ \frac{(I+1)(2I+1)(2I+3)J(J+1)(2J+1)}{I(2I-1)(2J-1)(2J+3)} \right]^{1/2}, \quad (1)$$

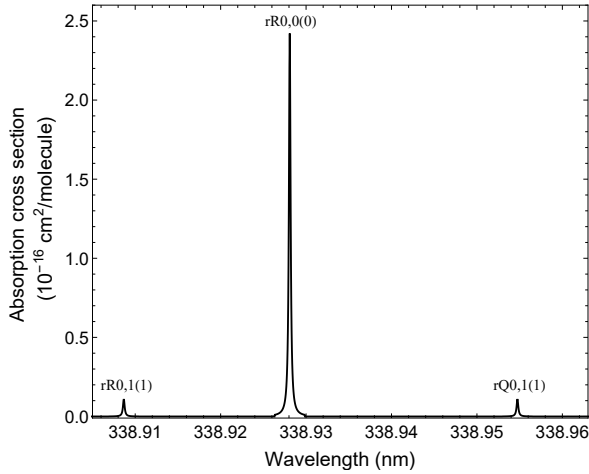


FIG. 4. Simulated absorption spectrum of the  $2_0^1 4_0^1$  vibronic band of formaldehyde, using Gaussian and Lorentzian FWHM of  $0.003 \text{ cm}^{-1}$  and  $0.02 \text{ cm}^{-1}$ , respectively, and  $T = 1 \text{ K}$ . Relevant transitions are labeled. The absorption spectrum simulation of the  $2_0^1 4_0^1$  vibronic band was performed using the PGOHER [47] program and the supporting material provided by [48].

where  $I = 1$  is the sum of proton spins,  $J$  the rotational angular momentum,  $F = J + I$  the total angular momentum,  $C$  the spin-rotation interaction constant and  $D$  the spin-spin interaction constant. Substituting  $C(1_{11}) = -3.07 \text{ kHz}$  and  $D(1_{11}) = 8.87 \text{ kHz}$  [46] for the lower state  $K_1 = 1$  we obtain the hamiltonian matrix elements in the  $|F, m_F\rangle$  representation. After transforming to the  $|m_J, m_I\rangle$  basis as:

$$|m_J, m_I\rangle = \sum_{F, m_F} \langle F, m_F | m_J, m_I \rangle |F, m_F\rangle, \quad (2)$$

the hamiltonian is diagonalized to obtain the time evolved states [34] shown in Fig. 3, where at  $t_{max} = 16.2 \mu\text{s}$ , 15.9% of the population has been transferred to the  $m_J = -1$  state, which is always fully nuclear-spin-polarized (Fig. 3(b)). The  $\langle m_I \rangle$  of each  $m_J$  state is plotted (Fig. 3(c,d)), giving the degree of nuclear polarization for each state.

The same technique can be applied to singly deuterated formaldehyde, CHDO. The effective hyperfine hamiltonian for asymmetric top molecules with two (nonzero) nuclear spins is written as [49]:

$$\begin{aligned} H/h = & \frac{(eq_J Q)_D}{2I_D(2I_D - 1)J(2J - 1)} \left[ 3(\vec{I}_D \cdot \vec{J})^2 + \frac{3}{2}(\vec{I}_D \cdot \vec{J}) \right. \\ & \left. - \vec{I}_D^2 \vec{J}^2 \right] + \frac{d'_J}{J(2J - 1)} \left[ \frac{3}{2}(\vec{I}_D \cdot \vec{J})(\vec{I}_H \cdot \vec{J}) \right. \\ & \left. + \frac{3}{2}(\vec{I}_H \cdot \vec{J})(\vec{I}_D \cdot \vec{J}) - (\vec{I}_H \cdot \vec{I}_D) \vec{J}^2 \right] \\ & + C_H \vec{I}_H \cdot \vec{J} + C_D \vec{I}_D \cdot \vec{J}, \end{aligned} \quad (3)$$

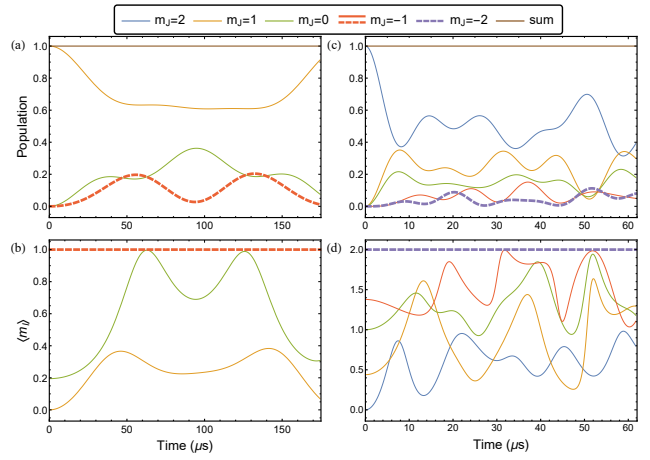


FIG. 5.  $\text{CH}_2\text{O}_2$  (a,b): Population and total  $\langle m_I \rangle$  of  $m_J$  states as function of time. The  $m_J = -1$  state reaches 10% of the total population at  $33 \mu\text{s}$ .  $\text{CD}_2\text{O}_2$  (c,d): Population and total  $\langle m_I \rangle$  of  $m_J$  states as function of time. The  $m_J = -2$  state reaches 8.8% of the total population at  $\sim 20 \mu\text{s}$ .

where  $(eq_J Q)_D$ ,  $d'_J$ ,  $C_H$ , and  $C_D$  are the quadrupole interaction coupling constant, the nuclear spin-spin interaction coupling constant, the proton and deuteron spin-rotation interaction coupling constants, defined in [49].

The hyperfine structure of the  $1_{11}$  and  $1_{10}$  states of CHDO has been studied by Tucker et al. [50]. We investigate the polarization dynamics of the  $1_{10}$ . Substituting  $C_H = -1.43 \text{ kHz}$ ,  $C_D = 0.11 \text{ kHz}$  given in [50],  $d'_J = -0.54 \text{ kHz}$  which is calculated from molecular geometry (as it is presented in Fig. 2 of [51]), and  $(eq_J Q)_D = 17 \text{ kHz}$ , where the  $\chi_{aa}$ ,  $\chi_{bb}$ , and  $\chi_{cc}$  are taken from Table V of [51]. Following the polarization scheme presented in Fig. 2(a), we achieve 21.4% of population with 100% deuteron polarization at  $7.9 \mu\text{s}$  (see Fig. 3(c,d)).

To produce nuclear-spin-polarized HD or DT molecules, a different scheme (Fig. 2) is required. Starting with  $m_J = 2$  ( $t=0$ ), at time  $t=t_{max}$  the population of the  $m_J = -1$  state is maximized (which has 100% nuclear-spin-polarization), and is then excited to the  $J=1$ ,  $m_J = +1$  state. For the calculation of  $t_{max}$  the hyperfine constants for the  $J=2$  state are needed. However, the  $C_{H,D}$  values found in the literature [49–51] are not consistent and the  $M_{gg}^{H,D}$  have not been measured. Thus, we cannot accurately determine  $t_{max}$  unless all the hyperfine constants of CHDO are known. The proton spin-rotation constants are particularly required, because they are mainly responsible for the polarization transfer to the proton. In the case of D, the corresponding quadrupole coupling interaction is dominating.

Similar methods can be applied to ortho-trans-formic acid and isotopes. The effective hyperfine hamiltonian of

formic acid ( $\text{CH}_2\text{O}_2$ ) is written as [49, 52, 53]:

$$H/h = C_{H_1} \vec{I}_1 \cdot \vec{J} + C_{H_2} \vec{I}_2 \cdot \vec{J} + \frac{d'_J}{J(2J-1)} \left[ \frac{3}{2} (\vec{I}_1 \cdot \vec{J})(\vec{I}_2 \cdot \vec{J}) + \frac{3}{2} (\vec{I}_2 \cdot \vec{J})(\vec{I}_1 \cdot \vec{J}) - (\vec{I}_1 \cdot \vec{I}_2) J^2 \right], \quad (4)$$

where  $I_1 = I_2 = 1/2$ ,  $d'_J = -\frac{6\mu_N^2 g_H^2}{(J+1)(2J+3)r^3} \sum_g \frac{r_g^2}{r^2} \langle J_g^2 \rangle - \frac{1}{3} J(J+1)$ ,  $C_{H_{1,2}} = \sum_g \frac{M_{gg}^{1,2} \langle J_g^2 \rangle}{J(J+1)}$ , and the constants labeled with 1 refer to the proton bounded to the carbon atom. For the  $1_{11}$  state,  $C_{H_1} = -3.8$  kHz,  $C_{H_2} = -4.1$

kHz [53], and  $d'_J = 1.8$  kHz [54, 55]. Figure 5 shows that the population of the  $m_J = -1$  state reaches 10% at  $t \sim 33$   $\mu\text{s}$ , assuming 100% rotational polarization at  $t = 0$ .

The same technique, but for the  $|\nu', J = 2\rangle$  state (Fig. 2(b)) can be applied to double deuterated formic acid ( $\text{CD}_2\text{O}_2$ ). The total wavefunction is symmetric in the exchange of nuclear spins  $I_1$  and  $I_2$ . In the case of  $K_{-1} = \text{even}$  states, the rotation wavefunction is symmetric, so the nuclear spin wavefunction must be symmetric, i.e.  $I = I_1 + I_2 = 0, 2$  (ortho states). Therefore, the non-zero hamiltonian matrix elements in the  $|J, I, F\rangle$  representation are [51]:

$$\begin{aligned} \langle J, I, F | H/h | J, I, F \rangle &= C_D \frac{A}{2J(J+1)} + \left[ a_Q \frac{3I(I+1) - 11}{(2I-1)(2I+3)} + a_S \frac{I(I+1) + 8}{2(2I-1)(2I+3)} \right] \frac{3A(A-1) - 4I(I+1)J(J+1)}{2J(J+1)(2J-1)(2J+3)}, \\ \langle J, I, F | H/h | J, I-2, F \rangle &= \frac{3(2a_Q - a_S)}{8J(J+1)(2J-1)(2J+3)(2I-1)} \sqrt{\frac{(I+3)(3-I)(I+2)(4-I)}{(2I-3)(2I+1)}} [(J-F+I)(J+F+I+1) \\ &\quad \times (F+I-J)(J+F-I+1)(J-F+I-1)(J+F+I)(F+I-1-J)(J+F-I+2)]^{1/2}, \end{aligned} \quad (5)$$

where  $A = J(J+1) + I(I+1) - F(F+1)$ . The constants  $a_Q$ ,  $a_S$ , and  $C_D$  are the quadrupole interaction coupling constant, the nuclear spin-spin interaction coupling constant, and the spin-rotation interaction coupling constant, defined in [51].

Cazzoli et al. [56] measured the hyperfine constants  $\chi_{gg}$  and calculated  $M_{gg}$  (see cc-pCVQZ calculation) using a semi-experimental equilibrium geometry. Figure 5(c,d) shows the hyperfine beats of the  $2_{21}$  state which is initially rotationally polarized. The values of the hyperfine constants are  $a_Q = -152.85$  kHz,  $a_S = 0.24$  kHz, and  $C_D = -2.85$  kHz. The 8.8% of the population has been transferred to the  $m_J = -2$  state, at  $t_{max} = 20$   $\mu\text{s}$ . This state is always fully nuclear-spin-polarized (Fig. 5(c,d)).

This method of macroscopic production of polarized molecules can be generalized to several other systems, such as for spin-polarized  $\text{O}_2$ ,  $\text{N}_2$ ,  $\text{NO}$ , and  $^{13}\text{CO}$ , from the IR-excitation and photodissociation of  $\text{O}_3$ ,  $\text{N}_2\text{O}$ ,  $\text{NO}_2$ , and  $\text{CO}_2$ .

This work is supported in part by the Hellenic Foundation for Research and Innovation (HFRI) and the General Secretariat for Research and Technology (GSRT), through the grant agreement No. HFRI-FM17-3709 (project NUPOL).

- 
- [2] R. A. Green, R. W. Adams, S. B. Duckett, R. E. Mewis, D. C. Williamson, and G. G. Green, *Prog. Nucl. Mag. Res. Sp.* **67**, 1 (2012).
  - [3] K. R. Keshari and D. M. Wilson, *Chem. Soc. Rev.* **43**, 1627 (2014).
  - [4] M. H. Levitt, *Annu. Rev. Phys. Chem.* **63**, 89 (2012).
  - [5] E. ter Haar and W. G. Clark, *J. Low Temp. Phys.* **94**, 361 (1994).
  - [6] G. Hupin, S. Quaglioni, and P. Navrátil, *Nat. Commun.* **10**, 351 (2019).
  - [7] M. Temporal, V. Brandon, B. Canaud, J. Didelez, R. Fedosejevs, and R. Ramis, *Nucl. Fusion* **52**, 103011 (2012).
  - [8] K. Grigoryev, N. Chernov, R. Engels, I. Ivanov, S. Kiselev, E. Komarov, L. Kotchenda, P. Kravtsov, L. Kroell, A. Martyushov, M. Marusina, M. Mikirtychyants, N. Nikolaev, F. Rathmann, H. P. gen Schieck, S. Sherman, H. Ströher, V. Trofimov, A. Vasilyev, and M. Vznuzdaev, *J. Phys. Conf.* **295**, 012168 (2011).
  - [9] R. M. Kulsrud, *Application of polarized nuclei to fusion, in Muon-Catalyzed Fusion and Fusion with Polarized Nuclei*, edited by B. Brunelli and G. G. Leotta (Springer US, Boston, MA, 1987) pp. 169–178.
  - [10] R. W. Moir, *Fusion Technol.* **21**, 1475 (1992).
  - [11] J. H. Ardenkjaer-Larsen, B. Fridlund, A. Gram, G. Hansson, L. Hansson, M. H. Lerche, R. Servin, M. Thaning, and K. Golman, *Proc. Natl. Acad. Sci. USA* **100**, 10158 (2003).
  - [12] A. C. Pinon, A. Capozzi, and J. H. Ardenkjaer-Larsen, *Commun. Chem.* **3**, 57 (2020).
  - [13] Y. Shestakov, D. Nikolenko, I. Rachek, D. Toporkov, and A. Yurchenko, *Phys. Part. Nuclei* **50**, 513 (2019).
  - [14] T. Kravchuk, M. Reznikov, P. Tichonov, N. Avidor, Y. Meir, A. Bekkerman, and G. Alexandrowicz, *Science* **331**, 319 (2011).

---

\* ptr@iesl.forth.gr

[1] E. Steffens and W. Haeberli, *Rep. Prog. Phys.* **66**, 1887 (2003).

- [15] D. A. Horke, Y.-P. Chang, K. Długołęcki, and J. Küpper, *Angew. Chem. Int. Ed.* **53**, 11965 (2014).
- [16] T. P. Rakitzis, *Phys. Rev. Lett.* **94**, 083005 (2005).
- [17] L. Rubio-Lago, D. Sofikitis, A. Koubenakis, and T. P. Rakitzis, *Phys. Rev. A* **74**, 042503 (2006).
- [18] D. Sofikitis, L. Rubio-Lago, M. R. Martin, Davida J. Ankeny Brown, Nathaniel C.-M. Bartlett, R. N. Zare, and T. P. Rakitzis, *Phys. Rev. A* **76**, 012503 (2007).
- [19] D. Sofikitis, L. Rubio-Lago, M. R. Martin, D. J. Ankeny Brown, N. C.-M. Bartlett, A. J. Alexander, R. N. Zare, and T. P. Rakitzis, *J. Chem. Phys.* **127**, 144307 (2007).
- [20] R. Engels, M. Gaißer, R. Gorski, K. Grigoryev, M. Mikirtychyants, A. Nass, F. Rathmann, H. Seyfarth, H. Ströher, P. Weiss, L. Kochenda, P. Kravtsov, V. Trofimov, N. Tschernov, A. Vasilyev, M. Vznuzdaev, and H. P. g. Schieck, *Phys. Rev. Lett.* **115**, 113007 (2015).
- [21] S. B. Mirov, I. S. Moskalev, S. Vasilyev, V. Smolski, V. V. Fedorov, D. Martyskhin, J. Peppers, M. Mirov, A. Der-gachev, and V. Gapontsev, *IEEE J. Sel. Top. Quantum Electron.* **24**, 1 (2018).
- [22] A. G. Suits, S. D. Chambreau, and S. A. Lahankar, *Int. Rev. Phys. Chem.* **26**, 585 (2007).
- [23] Y. Ma, J. Liu, F. Li, F. Wang, and T. N. Kitsopoulos, *J. Phys. Chem. A* **123**, 3672 (2019).
- [24] U. Even, J. Jortner, D. Noy, N. Lavie, and C. Cossart-Magos, *J. Chem. Phys.* **112**, 8068 (2000).
- [25] G. T. Fraser, L.-H. Xu, R. D. Suenram, and C. L. Lugez, *J. Chem. Phys.* **112**, 6209 (2000).
- [26] G. T. Fraser, R. D. Suenram, and C. L. Lugez, *J. Phys. Chem. A* **105**, 9859 (2001).
- [27] D. H. Levy, *Science* **214**, 263 (1981).
- [28] K. Bergmann, H.-C. Nägerl, N. Panda, G. Gabrielse, E. Miloglyadov, M. Quack, G. Seyfang, G. Wichmann, S. Ospelkaus, A. Kuhn, S. Longhi, A. Szameit, P. Pirro, B. Hillebrands, X.-F. Zhu, J. Zhu, M. Drewsen, W. K. Hensinger, S. Weidt, T. Halfmann, H.-L. Wang, G. S. Paraoanu, N. V. Vitanov, J. Mompert, T. Busch, T. J. Barnum, D. D. Grimes, R. W. Field, M. G. Raizen, E. Narevicius, M. Auzinsh, D. Budker, A. Pálffy, and C. H. Keitel, *J. Phys. B: At. Mol. Opt. Phys.* **52**, 202001 (2019).
- [29] N. V. Vitanov, A. A. Rangelov, B. W. Shore, and K. Bergmann, *Rev. Mod. Phys.* **89**, 015006 (2017).
- [30] K. Bergmann, N. V. Vitanov, and B. W. Shore, *J. Chem. Phys.* **142**, 170901 (2015).
- [31] N. C.-M. Bartlett, D. J. Miller, R. N. Zare, A. J. Alexander, D. Sofikitis, and T. P. Rakitzis, *Phys. Chem. Chem. Phys.* **11**, 142 (2009).
- [32] N. C.-M. Bartlett, J. Jankunas, R. N. Zare, and J. A. Harrison, *Phys. Chem. Chem. Phys.* **12**, 15689 (2010).
- [33] L. F. Phillips, *Chem. Phys. Lett.* **291**, 94 (1998).
- [34] C. S. Kannis, G. E. Katsoprinakis, D. Sofikitis, and T. P. Rakitzis, *Phys. Rev. A* **98**, 043426 (2018).
- [35] D. Singleton, G. Paraskevopoulos, and R. Irwin, *J. Photochem.* **37**, 209 (1987).
- [36] S. Maeda, T. Taketsugu, K. Ohno, and K. Morokuma, *J. Am. Chem. Soc.* **137**, 3433 (2015).
- [37] T. J. Butenhoff, K. L. Carleton, and C. B. Moore, *J. Chem. Phys.* **92**, 377 (1990).
- [38] R. Engels, H. Awwad, K. Grigoryev, L. Huxold, M. Martić, A. Rolofs, W. Sartison, H. Ströher, M. Büscher, A. Vasilyev, L. Kochenda, P. Kravtsov, V. Trofimov, and M. Vznudaev, *PoS PSTP2017*, 033 (2018).
- [39] T. R. Govers, L. Mattera, and G. Scoles, *J. Chem. Phys.* **72**, 5446 (1980).
- [40] A. Nass, C. Baumgarten, B. Braun, G. Ciullo, G. Court, P. Dalpiaz, A. Golendukhin, G. Graw, W. Haeberli, M. Henoch, R. Hertenberg, N. Koch, H. Kolster, P. Lenisa, H. Marukyan, M. Raithe, D. Reggiani, K. Rith, M. Simani, E. Steffens, J. Stewart, P. Tait, and T. Wise, *Nucl. Instrum. Meth. A* **505**, 633 (2003).
- [41] D. Sofikitis, P. Glodic, G. Koumarianou, H. Jiang, L. Bougas, P. C. Samartzis, A. Andreev, and T. P. Rakitzis, *Phys. Rev. Lett.* **118**, 233401 (2017).
- [42] D. Sofikitis, C. S. Kannis, G. K. Boulogiannis, and T. P. Rakitzis, *Phys. Rev. Lett.* **121**, 083001 (2018).
- [43] A. K. Spiliotis, M. Xygkis, M. E. Koutrakis, K. Tazes, G. K. Boulogiannis, C. S. Kannis, G. E. Katsoprinakis, D. Sofikitis, and T. P. Rakitzis, *Light Sci. Appl.* **10**, 35 (2021).
- [44] A. K. Spiliotis, M. Xygkis, M. Koutrakis, D. Sofikitis, and T. P. Rakitzis, *arXiv:2101.02675*.
- [45] P. C. Cross, R. M. Hainer, and G. W. King, *J. Chem. Phys.* **12**, 210 (1944).
- [46] S. Kukolich and D. Ruben, *J. Mol. Spectrosc.* **38**, 130 (1971).
- [47] C. M. Western, PGOPHER, a program for rotational, vibrational and electronic spectra, University of Bristol, 2005, <http://pgopher.chm.bris.ac.uk>.
- [48] C. A. Smith, F. D. Pope, B. Cronin, C. B. Parkes, and A. J. Orr-Ewing, *J. Phys. Chem. A* **110**, 11645 (2006).
- [49] P. Thaddeus, L. C. Krisher, and J. H. N. Loubser, *J. Chem. Phys.* **40**, 257 (1964).
- [50] K. Tucker and G. Tomasevich, *J. Mol. Spectrosc.* **48**, 475 (1973).
- [51] W. H. Flygare, *J. Chem. Phys.* **41**, 206 (1964).
- [52] J. Chardon, C. Genty, D. Guichon, and J. Theobald, *J. Chem. Phys.* **64**, 1437 (1976).
- [53] Cazzoli, G., Puzzarini, C., Stopkowicz, S., and Gauss, J., *A&A* **520**, A64 (2010).
- [54] J. Bellet, A. Deldalle, C. Samson, G. Stenbeckeliers, and R. Wertheimer, *J. Mol. Struct.* **9**, 65 (1971).
- [55] W. H. Hocking, *Z. Naturforsch. A* **31**, 1113 (1976).
- [56] G. Cazzoli, C. Puzzarini, S. Stopkowicz, and J. Gauss, *Chem. Phys. Lett.* **502**, 42 (2011).